

Three-dimensional graphdiyne as a topological nodal-line semimetal

Takafumi Nomura¹, Tetsuro Habe¹, Ryota Sakamoto² and Mikito Koshino¹

¹ Department of Physics, Osaka University, Toyonaka 560-0043, Japan and

² Department of Chemistry, The University of Tokyo, Tokyo 113-0033, Japan

(Dated: January 5, 2019)

We study the electronic band structure for three-dimensional graphdiyne, of which crystal structure was recently identified as ABC (rhombohedral) stacking. Using the first-principles calculation, we find that the ABC graphdiyne is a nodal-line semimetal, in which the conduction band and valence band cross on a closed ring in the momentum space. We find a minimum tight-binding model to approximate the first-principles band structure, and also obtain an low-energy effective Hamiltonian in a 4×4 matrix form. The nodal line is shown to be protected by a non-trivial winding number, and the associated surface state is found in a slab geometry. The Fermi surface in finite doping exhibits a peculiar, self-intersecting hourglass structure. Despite its simple constitution, ABC-stacked GDY offers unique electronic properties distinct from any other carbon allotropes.

Since the discovery of graphene [1], tremendous theoretical and experimental efforts have been paid to this alluring two-dimensional (2D) material, disclosing its breakthrough properties and innovative applications [2, 3]. In the other context, a series of 2D allotropes of carbon, graphyne, has been also pursued theoretically [4–6] to seek for novel carbon materials. Graphyne refers to a group of planar 2D carbon materials consisting of benzene rings (sp^2 carbons) and ethynyl bridges (sp). Among the graphyne series, it is only graphdiyne (GDY) [7] [Fig. 2(b)] that was realized experimentally [8]. GDY may be synthesized by chemical polymerization of hexaethynylbenzene monomers. The experimentally fabricated GDY takes a form of 3D stack of 2D layers [8–12]. Various applications have been proposed for bulk GDY [10–12], however, its stack structure was not elucidated. In 2017, one of the authors has produced a high-quality GDY nanosheet, and identified its structure as ABC (rhombohedral) stacking [13] [Fig. 2(a)].

In theories, the electronic property was studied for various GDY-based systems [5, 14–23]. The band calculation for monolayer GDY predicted a semiconducting band gap [5, 14, 15], while the bulk ABC-stacked GDY has not yet been investigated theoretically. In this letter, we theoretically explore the electronic structure of three-dimensional ABC-stacked GDY by the first-principles calculation and the effective mass theory. We identified the system as a nodal-line semimetal [24–27], in which the conduction band and valence band cross at a closed ring in the momentum space [Fig. 1(a)]. We obtain a minimum tight-binding model and an low-energy effective Hamiltonian to approximate the band structure. Using the effective model, we prove the topological protection of the nodal line as well as the existence of the topological surface states. We also show that the Fermi surface of the doped system exhibits a peculiar self-intersecting hourglass shape as illustrated in Fig. 1(b).

The atomic structure of ABC-stacked GDY is illustrated in Fig. 2(a). The structure is rhombohedral [13] with lattice vectors $\mathbf{a}_1 = (0, L/\sqrt{3}, d)$, $\mathbf{a}_2 =$

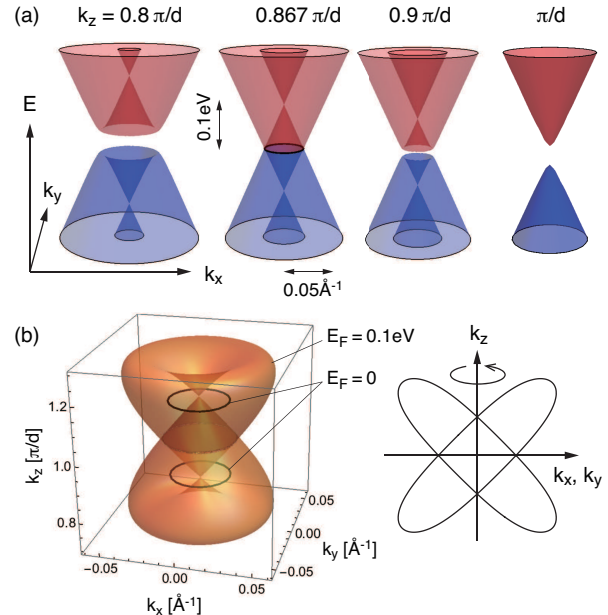


FIG. 1. (a) Energy band structure of 4×4 effective model for ABC-stacked GDY, plotted against (k_x, k_y) at various fixed k_z 's. (b) Fermi surface for $E_F = 0.1$ eV and the nodal lines for $E_F = 0$ in the effective model. The right panel is its cross section of the $E_F = 0.1$ eV surface.

$(-L/2, -L/(2\sqrt{3}), d)$ and $\mathbf{a}_3 = (L/2, -L/(2\sqrt{3}), d)$, where L is the lattice constant of single layer GDY and d is the interlayer spacing. A unit cell consists of 18 carbon atoms as shown in Fig. 2(b), where a benzene ring at the center is connected to six neighboring cells by linear chains. As shown later, the distances between neighboring carbon atoms slightly differ depending on the positions, and they are labeled as b_i ($i = 1, 2, 3, 4$) as indicated in Fig. 2(b).

We perform the first-principles density function theory (DFT) calculation using the numerical package of quantum-ESPRESSO [28] to obtain the electronic structure of three-dimensional ABC-stacked GDY. Here

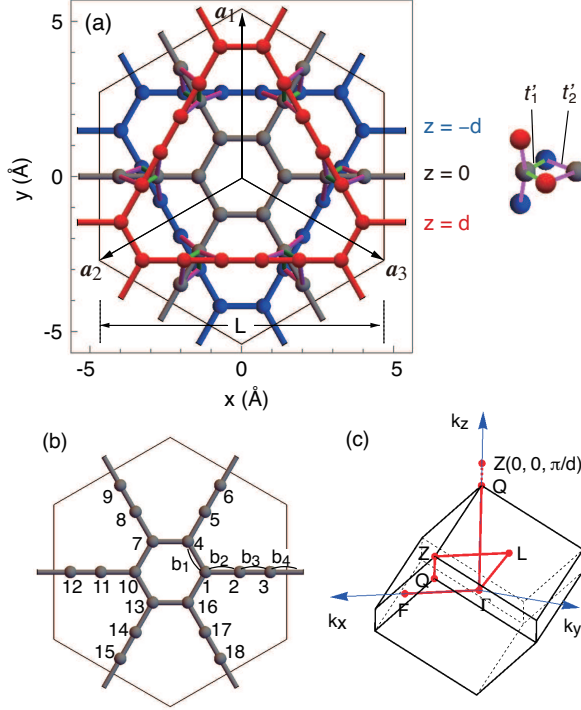


FIG. 2. (a) Stacking structure of ABC-stacked GDY projected on xy -plane. (b) A unit cell with numbering of the atoms. (c) Brillouin zone. The same symbols represent the equivalent point.

we employ the ultrasoft pseudopotentials with Perdew-Zunger self-interaction corrected density functional, the cutoff energy of the plane-wave basis 60 Ry, and the convergence criterion of 10^{-8} Ry in $12 \times 12 \times 12$ wave number mesh. In the calculation, the lattice structure and atomic positions are optimized by structural relaxation code in quantum-ESPRESSO. Here the criterion for the structural relaxation for total energy convergence is taken as 10^{-4} Ry in $6 \times 6 \times 6$ wave number mesh, and that for force on atoms is taken as 10^{-3} Ry/ a_B with Bohr radius a_B .

In the optimized structure, we have $L = 9.38\text{\AA}$, $d = 3.29\text{\AA}$, $b_1 = 1.42\text{\AA}$, $b_2 = 1.38\text{\AA}$, $b_3 = 1.23\text{\AA}$, and $b_4 = 1.33\text{\AA}$, and there is no out-of-plane distortion. Figure 3(a) presents the calculated band structure of the ABC-stacked GDY on the k -space path indicated in Figure 2(c). We find that the interlayer coupling significantly reduces the energy gap of monolayer, and the energy bands are nearly touching at Z point, or $(0, 0, \pi/d)$. The band crossing is actually located at off-symmetric point near Z . Figure 4(a) shows the band dispersion along the in-plane direction (k_x) at several fixed k_z 's from 0 to π/d , and (b) is the further detailed plot near zero energy. At $k_z = \pi/d$, we have nearly two-fold degenerate bands in each of the conduction and the valence sectors. When the k_z shifts away from π/d , the degeneracy splits

and the middle two bands touch in $k_z \approx 0.862\pi/d$, at some off-center in-plane momentum k_x . The low-energy band structure is nearly circular symmetric with respect to k_z axis, so that we have band touching along a ring on $k_x k_y$ plane. The nodal ring is slightly distorted in 120° symmetry, and also disperses in energy with the width ~ 1 meV.

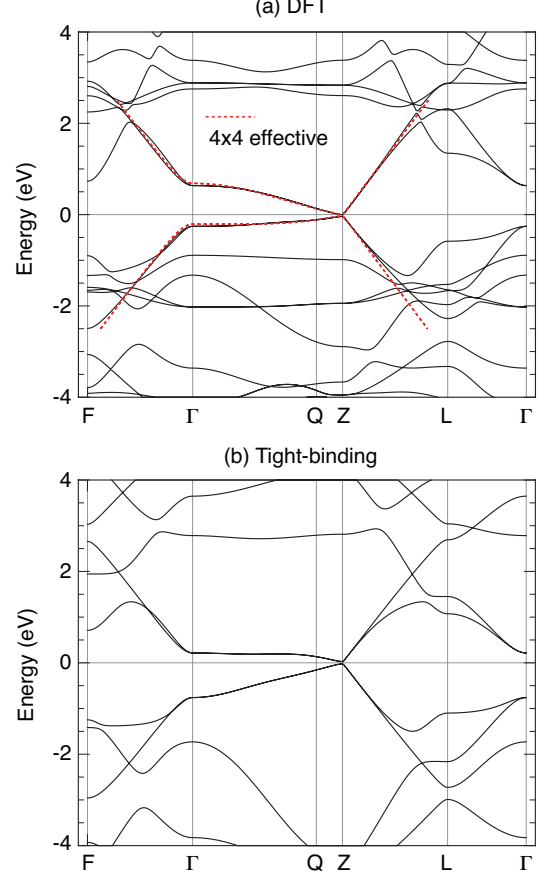


FIG. 3. (a) DFT-calculated band structure of ABC-stacked GDY on the k -space path indicated in Fig. 2(c). Red dashed curves are the band of the 4×4 effective model Eq. (4). (b) Corresponding band structure of the tight-binding model.

Since the low-energy band structure of GDY is dominated by p_z orbital [5], it can be described by the single band tight-binding model. Here we construct a simple tight-binding Hamiltonian to describe ABC-stacked GDY by considering the major hopping integrals only. For the intralayer coupling, we take the nearest neighboring hoppings t_i ($i = 1, 2, 3, 4$), which correspond to the distance b_i ($i = 1, 2, 3, 4$), respectively. For the interlayer coupling, we take the two shortest, nearly vertical bonds of 3.34\AA and 3.38\AA , and define the corresponding hopping integrals as t'_1 and t'_2 , respectively [Fig. 2(a)]. To obtain the transfer integral of those selected bonds, we adopt the Slater-Koster type formula used for carbon

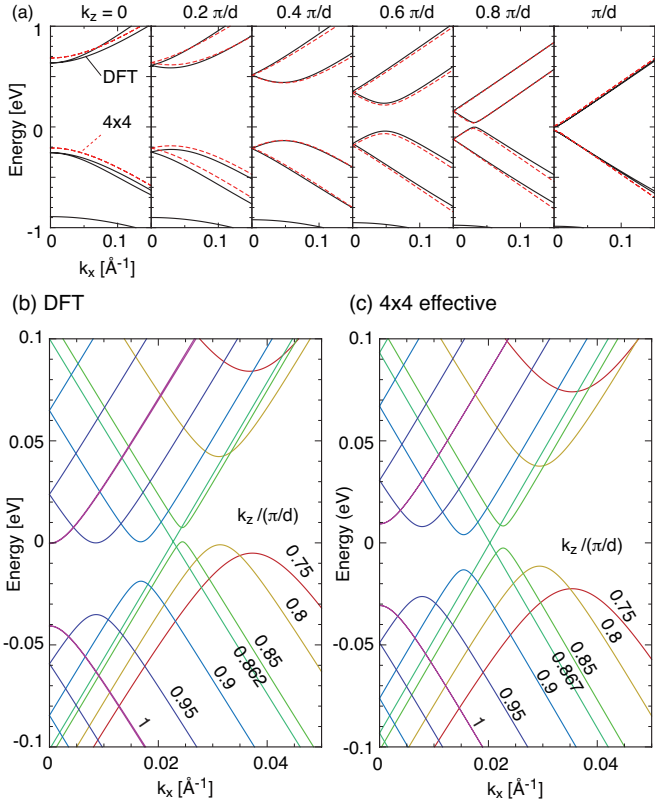


FIG. 4. (a) Low-energy band structure of ABC-stacked GDY plotted against k_x . Black solid and red dashed curves indicate the DFT and the 4×4 effective model Eq. (4), respectively. (b) Magnified plot near the band closing point for DFT (left) and the effective model (right).

p_z -orbitals in graphene [29–32],

$$-t(\mathbf{R}) = V_{pp\pi} \left[1 - (\hat{\mathbf{R}} \cdot \mathbf{e}_z)^2 \right] + V_{pp\sigma} (\hat{\mathbf{R}} \cdot \mathbf{e}_z)^2, \\ V_{pp\pi} = V_{pp\pi}^0 e^{-(R-a_0)/r_0}, \quad V_{pp\sigma} = V_{pp\sigma}^0 e^{-(R-d_0)/r_0}. \quad (1)$$

Here \mathbf{R} is the distance between two atoms, $\hat{\mathbf{R}} = \mathbf{R}/R$ and \mathbf{e}_z is the unit vector on z axis. $V_{pp\pi}^0 \approx -2.7$ eV is the transfer integrals between nearest-neighbor atoms of monolayer graphene which are located at distance $a_0 = a/\sqrt{3} \approx 0.142$ nm. $V_{pp\sigma}^0 \approx 0.48$ eV is the transfer integral between two nearest-vertically aligned atoms and $d_0 \approx 0.334$ nm is the interlayer spacing of graphite. The parameter r_0 , the decay length of transfer integral is chosen as 0.09 nm. The hopping parameters are then obtained as $t_1 = 2.71$ eV, $t_2 = 2.82$ eV, $t_3 = 3.34$ eV, $t_4 = 2.99$ eV, $t'_1 = 0.463$ eV, $t'_2 = 0.421$ eV. Figure 3(b) presents the band structure of the tight-binding model. By comparing with the DFT band structure in Fig. 3(a), we actually see that the qualitative features of low-energy bands are well reproduced.

Finally we derive the effective continuum Hamiltonian for the low-energy spectrum. At Γ -point, we define four

bases by

$$|\psi_1\rangle = (i/\sqrt{18})(1, 1, -1, \omega, \omega, -\omega, \omega^*, \omega^*, -\omega^* \\ 1, 1, -1, \omega, \omega, -\omega, \omega^*, \omega^*, -\omega^*), \\ |\psi_2\rangle = (i/\sqrt{18})(1, 1, -1, \omega^*, \omega^*, -\omega^*, \omega, \omega, -\omega, \\ 1, 1, -1, \omega^*, \omega^*, -\omega^*, \omega, \omega, -\omega), \\ |\psi_3\rangle = (1/\sqrt{18})(1, -1, -1, -\omega, \omega, \omega, \omega^*, -\omega^*, -\omega^*, \\ -1, 1, 1, \omega, -\omega, -\omega, -\omega^*, \omega^*, \omega^*), \\ |\psi_4\rangle = (1/\sqrt{18})(1, -1, -1, -\omega^*, \omega^*, \omega^*, \omega, -\omega, -\omega, \\ -1, 1, 1, \omega^*, -\omega^*, -\omega^*, -\omega, \omega, \omega), \quad (2)$$

where $\omega = e^{2\pi i/3}$, and the vector components represent the wave amplitudes of the site 1 to 18 in the unit cell numbered in Fig. 2(b). The four bases are eigenstates of space inversion with parity + for ψ_1, ψ_2 and - for ψ_3, ψ_4 . They are also eigenstates 120° rotation with eigenvalue ω for ψ_1, ψ_3 and ω^* for ψ_2, ψ_4 . The time-reversal operation relates the bases as $\psi_1 = -\psi_2^*$ and $\psi_3 = \psi_4^*$. The reflection $R_x[(x, y, z) \rightarrow (-x, y, z)]$ operates as $R_x\psi_1 = \psi_2$ and $R_x\psi_3 = -\psi_4$. The bases at general k -points are defined by multiplying ψ_i by the Bloch factor $e^{i\mathbf{k} \cdot \mathbf{r}}$ for every lattice point \mathbf{r} .

We set our basis as $U = (|\psi_1\rangle, |\psi_2\rangle, |\psi_3\rangle, |\psi_4\rangle)$ and obtain the reduced 4×4 Hamiltonian by calculating the matrix $U^\dagger H U$ with the tight-binding Hamiltonian H . Then we expand the matrix in terms of in-plane wave number (k_x, k_y) , and obtain the effective low-energy Hamiltonian. For the single layer GDY, the Hamiltonian within the linear order of (k_x, k_y) becomes

$$H_{\text{mono}} = \begin{pmatrix} \Delta & 0 & 0 & \hbar v k_- \\ 0 & \Delta & \hbar v k_+ & 0 \\ 0 & \hbar v k_- & -\Delta & 0 \\ \hbar v k_+ & 0 & 0 & -\Delta \end{pmatrix} \quad (3)$$

where $k_\pm = k_x \pm ik_y$, $\Delta = (t_1 - 2t_2 + 2t_3 - t_4)/3$, $v = (2t_1 + 2t_2 + 2t_3 + t_4)b/(6\hbar)$, and b is the average of neighboring bond lengths $b_1 \dots b_4$. It is equivalent with the two-dimensional Dirac Hamiltonian with the mass parameter Δ and the light velocity replaced with v . The mass gap Δ is sensitive to the difference among the interlayer hopping parameters t_1, \dots, t_4 ; if they were all the identical, Δ vanishes and the spectrum would be gapless.

The Hamiltonian of ABC-stacked GDY is derived in a similar manner as

$$H_{\text{ABC}} = \begin{pmatrix} \epsilon_0 + m & 0 & -ib & \hbar v k_- \\ 0 & \epsilon_0 + m & \hbar v k_+ & ib \\ ib & \hbar v k_- & \epsilon_0 - m & 0 \\ \hbar v k_+ & -ib & 0 & \epsilon_0 - m \end{pmatrix}, \\ \epsilon_0(k_z) = u_0 \cos(k_z d), \quad m(k_z) = \Delta + u_1 \cos(k_z d), \\ b(k_z) = u_2 \sin(k_z d). \quad (4)$$

Here u_0, u_1 and u_2 describe the interlayer coupling, and they are related by the tight-binding hoppings as $u_0 =$

$-t'_1/3$, $u_1 = 2t'_2/3$ and $u_2 = -t'_1/\sqrt{3}$. Δ and v are just as defined for monolayer. We can show that the nearest-neighbor interlayer Hamiltonian for the basis of Eq. (2) is required to have the above form within zero-th order in k_x and k_y , only by considering the symmetries mentioned above. There u_0 , u_1 and u_2 are free parameters.

The five parameters (v, Δ, u_0, u_1, u_2) of H_{ABC} can be determined directly to fit the DFT band structure. Our best fit is $v \approx 7.1 \times 10^5$ m/s, $\Delta = 0.213$ eV, $u_0 = 0.104$ eV, $u_1 = 0.233$ eV, and $u_2 = 0.230$ eV. In Fig. 3(a) and Fig. 4(a), the red dashed curves indicate the energy bands of the effective band model with those parameters, which fit quite well with the DFT band structure in the low energy region. We also show the detailed plot near zero energy in Fig. 4(c), where the band touching nature is also reproduced.

The eigenenergies of H_{ABC} is given by $E_{s,s'}(\mathbf{k}) = \epsilon_0 + s\sqrt{m^2 + (\hbar v k_{\parallel} + s'b)^2}$, where $s = \pm$, $s' = \pm$ and $k_{\parallel} = (k_x + k_y)^{1/2}$. The energy bands of $s = \pm$ touch only when $m(k_z) = 0$ and $\hbar v k_{\parallel} + s'b(k_z) = 0$, or equivalently, $k_z d = \pm \arccos(-\Delta/u_1)$ and $\hbar v k_{\parallel} = u_2 \sqrt{1 - \Delta^2/u_1^2}$. This determines the position of the nodal line. The real solution for (k_{\parallel}, k_z) exist when $|\Delta/u_1| \leq 1$, which is met in our system. The topological protection of the nodal line is checked by calculating the Berry phase along k_z axis at fixed in-plane momentum (k_x, k_y) . We define a unitary matrix,

$$V = \frac{1}{\sqrt{2}} \begin{pmatrix} 1 & 0 & 1 & 0 \\ -ie^{i\theta} & 0 & ie^{i\theta} & 0 \\ 0 & 1 & 0 & 1 \\ 0 & ie^{i\theta} & 0 & -ie^{i\theta} \end{pmatrix}, \quad (5)$$

where $\tan \theta = k_y/k_x$. Then the unitary transformed Hamiltonian $V^{\dagger} H_{ABC} V$ is block-diagonalized into two 2×2 matrices $H_{\pm} = Y\sigma_y + Z\sigma_z$, where $Y = \hbar v k_{\parallel} \pm b(k_z)$ and $Z = m(k_z)$, and σ_y and σ_z are the Pauli matrices. When k_z is changed from $-\pi/d$ to π/d , the trace of (Y, Z) encloses the origin only when $|\Delta/u_1| \leq 1$ and $\hbar v k_{\parallel} < u_2 \sqrt{1 - \Delta^2/u_1^2}$, so that the Berry phase is π only when the integral path passes through the nodal ring while 0 otherwise. Since the system has the time-reversal symmetry and the space inversion symmetry, the Berry curvature always vanishes at any nondegenerate points in the energy band [33, 34], and this guarantees the robustness of band touching against a small perturbation not to break these symmetries [35].

The nodal line also implies the existence of the topological surface states. Figure 5 shows the band structure calculated for the effective Hamiltonian with a finite thickness of 200 layers, plotted against k_x axis. We actually see that nearly-flat band originated from the surface modes appear between the nodal points. In (k_x, k_y) -space, the surface-state band spans the disk-shaped region inside the nodal ring.

When the Fermi energy is shifted from the nodal line

by electron or hole doping, the Fermi surface with a non-trivial structure emerges. Figure 1(b) shows the Fermi surface for $E_F = 0.1$ eV in the effective model. The figure is rotationally symmetric with respect to k_z axis, and its vertical cross section is presented in the right panel. The surface has a pair of conical points on k_z axis, at which the electron-like pocket and the hole-like pocket are connected. The surface is self-intersecting at $k_z = \pi/d$, and this corresponds to the degeneracy of the two conduction bands at $k_z = \pi/d$. In the higher Fermi energy, the energy bands and Fermi surface are trigonally warped in 120° symmetry, while the warping is irrelevant in $|E_F| < 0.1$ eV and neglected in the present effective model. We expect that the peculiar self-intersecting Fermi surface would cause unusual effects on the magnetotransport and optical properties through formation of the self-connected semiclassical orbits [36–38].

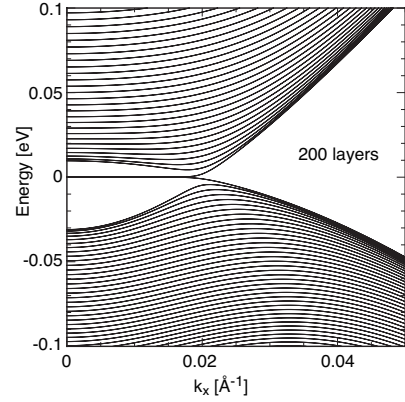


FIG. 5. Energy bands of ABC-stacked GDY with thickness of 200 layers

The spin-orbit coupling is entirely neglected in the present calculation. It tends to gap out the nodal line in the absence of non-symmorphic symmetry [27]. In carbon materials, however, the spin-orbit coupling is relatively small, and in particular, it is extremely weak in flat systems where π -band and σ -band are independent from each other [39]. For example, the spin-orbit energy scale is only 10 mK in graphene [39, 40]. A similar discussion may be applicable to GDY, a flat carbon π -system, and therefore the predicted nodal line should be preserved.

To conclude, we found that ABC-stacked GDY is a topological nodal semimetal by the DFT band calculation. We derive the minimal effective low-energy Hamiltonian and proved the topological protection of nodal line and also existence of the topological surface states. The Fermi surface of the doped systems exhibits a peculiar, self-intersecting hourglass shape. As purely carbon material with a plain structure, GDY would be one of the simplest topological nodal-line semimetals. Moreover, the graphyne family has an enormous variety of

derivatives with various geometric structures and atomic species [4, 17, 18, 20]. The discovery of topological nature of GDY not only sheds new light on carbon materials, but also broadens the physics of topological matters by offering a vast unexplored field.

M. K. and T. H. acknowledge support of JSPS KAKENHI Grant Numbers JP25107005, JP25107001 and JP17K05496. R. S. acknowledges support of JSPS KAKENHI Grant Numbers JP16H00900 and JP26708005, JST PRESTO Grant Number JPMJPR1516, Japan, the Asahi Glass Foundation, Kato foundation for Promotion of Science, the Murata Science Foundation, Yashima Environment Technology Foundation and Foundation Advanced Technology Institute.

[1] K. S. Novoselov, A. K. Geim, S. Morozov, D. Jiang, M. Katsnelson, I. Grigorieva, S. Dubonos, and A. Firsov, *Nature* **438**, 197 (2005).

[2] A. C. Neto, F. Guinea, N. M. Peres, K. S. Novoselov, and A. K. Geim, *Rev. Mod. Phys.* **81**, 109 (2009).

[3] M. J. Allen, V. C. Tung, and R. B. Kaner, *Chem. Rev.* **110**, 132 (2009).

[4] R. Baughman, H. Eckhardt, and M. Kertesz, *J. Chem. Phys.* **87**, 6687 (1987).

[5] N. Narita, S. Nagai, S. Suzuki, and K. Nakao, *Phys. Rev. B* **58**, 11009 (1998).

[6] N. Narita, S. Nagai, S. Suzuki, and K. Nakao, *Phys. Rev. B* **62**, 11146 (2000).

[7] M. M. Haley, S. C. Brand, and J. J. Pak, *Angewandte Chemie International Edition* **36**, 836 (1997).

[8] G. Li, Y. Li, H. Liu, Y. Guo, Y. Li, and D. Zhu, *Chem. Commun.* **46**, 3256 (2010).

[9] X. Qian, H. Liu, C. Huang, S. Chen, L. Zhang, Y. Li, J. Wang, and Y. Li, *Sci. Rep.* **5**, 7756 (2015).

[10] C. Kuang, G. Tang, T. Jiu, H. Yang, H. Liu, B. Li, W. Luo, X. Li, W. Zhang, F. Lu, *et al.*, *Nano lett.* **15**, 2756 (2015).

[11] Z. Jia, Y. Li, Z. Zuo, H. Liu, C. Huang, and Y. Li, *Acc. Chem. Res.* **50**, 2470 (2017).

[12] H. Shang, Z. Zuo, L. Li, F. Wang, H. Liu, Y. Li, and Y. Li, *Angew. Chem. Int. Ed.* **57**, 774 (2018).

[13] R. Matsuoka, R. Sakamoto, K. Hoshiko, S. Sasaki, H. Matsunaga, K. Nagashio, and H. Nishihara, *J. Am. Chem. Soc.* **139**, 3145 (2017).

[14] M. Long, L. Tang, D. Wang, Y. Li, and Z. Shuai, *ACS nano* **5**, 2593 (2011).

[15] G. Luo, X. Qian, H. Liu, R. Qin, J. Zhou, L. Li, Z. Gao, E. Wang, W.-N. Mei, J. Lu, *et al.*, *Phys. Rev. B* **84**, 075439 (2011).

[16] L. Pan, L. Zhang, B. Song, S. Du, and H.-J. Gao, *Appl. Phys. Lett.* **98**, 173102 (2011).

[17] S. W. Cranford, D. B. Brommer, and M. J. Buehler, *Nanoscale* **4**, 7797 (2012).

[18] K. Srinivasu and S. K. Ghosh, *J. Phys. Chem. C* **116**, 5951 (2012).

[19] Q. Zheng, G. Luo, Q. Liu, R. Quhe, J. Zheng, K. Tang, Z. Gao, S. Nagase, and J. Lu, *Nanoscale* **4**, 3990 (2012).

[20] Y. Li, L. Xu, H. Liu, and Y. Li, *Chem. Soc. Rev.* **43**, 2572 (2014).

[21] M. Hu, Y. Pan, K. Luo, J. He, D. Yu, and B. Xu, *Carbon* **91**, 518 (2015).

[22] L. Sun, P. Jiang, H. Liu, D. Fan, J. Liang, J. Wei, L. Cheng, J. Zhang, and J. Shi, *Carbon* **90**, 255 (2015).

[23] S. Jalili, F. Houshmand, and J. Schofield, *Appl. Phys. A* **119**, 571 (2015).

[24] A. A. Burkov, M. D. Hook, and L. Balents, *Phys. Rev. B* **84**, 235126 (2011).

[25] T. Habe and Y. Asano, *Phys. Rev. B* **89**, 115203 (2014).

[26] M. Phillips and V. Aji, *Phys. Rev. B* **90**, 115111 (2014).

[27] C. Fang, Y. Chen, H.-Y. Kee, and L. Fu, *Phys. Rev. B* **92**, 081201 (2015).

[28] P. Giannozzi, S. Baroni, N. Bonini, M. Calandra, R. Car, C. Cavazzoni, D. Ceresoli, G. L. Chiarotti, M. Cococcioni, I. Dabo, A. Dal Corso, S. de Gironcoli, S. Fabris, G. Fratesi, R. Gebauer, U. Gerstmann, C. Gougaoussis, A. Kokalj, M. Lazzeri, L. Martin-Samos, N. Marzari, F. Mauri, R. Mazzarello, S. Paolini, A. Pasquarello, L. Paulatto, C. Sbraccia, S. Scandolo, G. Sclauzero, A. P. Seitsonen, A. Smogunov, P. Umari, and R. M. Wentzcovitch, *J. Phys.: Condens. Matter* **21**, 395502 (2009).

[29] J. Slater and G. Koster, *Phys. Rev.* **94**, 1498 (1954).

[30] T. Nakanishi and T. Ando, *J. Phys. Soc. Jpn.* **70**, 1647 (2001).

[31] P. Moon and M. Koshino, *Phys. Rev. B* **85**, 195458 (2012).

[32] P. Moon and M. Koshino, *Phys. Rev. B* **87**, 205404 (2013).

[33] F. Haldane, *Phys. Rev. Lett.* **93**, 206602 (2004).

[34] L. Fu and C. L. Kane, *Phys. Rev. B* **76**, 045302 (2007).

[35] M. Koshino, *Phys. Rev. B* **88**, 115409 (2013).

[36] T. OBrien, M. Diez, and C. Beenakker, *Phys. Rev. Lett.* **116**, 236401 (2016).

[37] M. Koshino, *Phys. Rev. B* **94**, 035202 (2016).

[38] N. Bovenzi, M. Breitkreiz, T. OBrien, J. Tworzydlo, and C. Beenakker, *New J. Phys.* **20**, 023023 (2018).

[39] D. Huertas-Hernando, F. Guinea, and A. Brataas, *Phys. Rev. B* **74**, 155426 (2006).

[40] H. Min, J. Hill, N. A. Sinitsyn, B. Sahu, L. Kleinman, and A. H. MacDonald, *Phys. Rev. B* **74**, 165310 (2006).